UC Riverside
UC Riverside Previously Published Works

Title

Towards Patient-Specific 3D-Printed Robotic Systems for Surgical Interventions.

Permalink

https://escholarship.org/uc/item/35k553bf

Journal

IEEE Transactions on Medical Robotics and Bionics, 1(2)

Authors

Cheng, Shing

Wang, Xuefeng

Deaton, Nancy

et al.

Publication Date

2019-05-01

DOI

10.1109/tmrb.2019.2912444

Peer reviewed

Towards Patient-Specific 3D-Printed Robotic Systems for Surgical Interventions

Jaydev P. Desai[1] **[Fellow, IEEE]**, **Jun Sheng**[1] **[Student Member, IEEE]**, **Shing Shin Cheng**[2], **Xuefeng Wang**[3], **Nancy J. Deaton**[1], **Nahian Rahman**[1]

[1]J. P. Desai, J. Sheng, N. J. Deaton, and N. Rahman are with Medical Robotics and Automation (RoboMed) Laboratory in the Wallace H. Coulter Department of Biomedical Engineering, Georgia Institute of Technology, Atlanta, GA, 30332 USA.

[2]S. S. Cheng is with the Department of Mechanical and Automation Engineering, Chinese University of Hong Kong, Shatin, N.T. Hong Kong SAR, China.

[3]X. Wang is with the Department of Mechanical Engineering, University of Alabama, Tuscaloosa, AL, 35487, USA.

Abstract

Surgical robots have been extensively researched for a wide range of surgical procedures due to the advantages of improved precision, sensing capabilities, motion scaling, and tremor reduction, to name a few. Though the underlying disease condition or pathology may be the same across patients, the intervention approach to treat the condition can vary significantly across patients. This is especially true for endovascular interventions, where each case brings forth its own challenges. Hence it is critical to develop patient-specific surgical robotic systems to maximize the benefits of robot-assisted surgery. Manufacturing patient-specific robots can be challenging for complex procedures and furthermore the time required to build them can be a challenge. To overcome this challenge, additive manufacturing, namely 3D-printing, is a promising solution. 3D-printing enables fabrication of complex parts precisely and efficiently. Although 3D-printing techniques have been researched for general medical applications, patient-specific surgical robots are currently in their infancy. After reviewing the state-of-the-art in 3D-printed surgical robots, this paper discusses 3D-printing techniques that could potentially satisfy the stringent requirements for surgical interventions. We also present the accomplishments in our group in developing 3D-printed surgical robots for neurosurgical and cardiovascular interventions. Finally, we discuss the challenges in developing 3D-printed surgical robots and provide our perspectives on future research directions.

Index Terms

Surgical robots; 3D-printing; patient-specific; 3D-printed actuators; 3D-printed sensors; biocompatibility; sterilizability; smoothness; accuracy; thermal stability; stiffness; tendon-driven; shape memory alloy; neurosurgical robot; robotic catheter

---

jaydev@gatech.edu.

I. MOTIVATION

Since the first surgical robot was developed based on an industrial robot - PUMA 560 [1], surgical robots have been extensively researched and some of them have been commercialized [2]. So far, hundreds of thousands of robotic surgeries are performed annually and the number is steadily increasing by 25 percent annually [3]. Although open surgery provides a clear view of the surgical site, robot-assisted minimally invasive surgery brings about the benefits of smaller incision, reduced trauma, improved precision, and motion scaling (where necessary), which shortens hospital stay and overall cost of the procedure. For example, a flexible and steerable meso-scale robotic arm could maneuver inside the tissue and deliver local anesthetic safely without injury to adjacent organs or tearing large vessels [4].

Patient-specific minimally invasive surgical robotics is the trend of the future. Given the complexity as well as possible differences in the intervention approach across patients, such as different workspace volume, access to the intervention site, and the required motion capability, it is imperative to customize the surgical robot for improved patient outcomes, post surgery. For example, removal of deep intracranial brain tumor and spontaneous intracerebral hemorrhage are two examples of surgical interventions that can greatly benefit from patient-specific robots. To treat the lesion of different size and shape at different locations, the configuration of the surgical robot should be customized, such that it can reach the surgical site with minimal or no damage to any critical brain structures, while treating the vast majority of the lesion. Another example is intravascular procedures, which could benefit from a robotic catheter with customized bending capability to be able to smoothly pass through complex vasculature and reach the surgical target.

One approach to developing patient-specific surgical robots will require pre-operative imaging. Based on the imaging data, surgical robots can then be optimally designed taking into consideration, for example the motion planning requirements [5]. However, there are two primary challenges in fabricating a patient-specific surgical robot. Firstly, the lead time of fabricating a patient-specific robot should be short so as to reduce hospital stay and avoid the need to re-manufacture the robot, should there be any changes in the anatomy during the waiting period. Secondly, the fabrication of customized surgical robots should not be cost-prohibitive compared with standardized robotic tools for surgery. Thus, additive manufacturing, namely 3D-printing, emerges as a promising solution due to its relatively low cost and short fabrication period. 3D-printing enables us to develop customizable, complicated components with small features to develop lightweight and compact systems. Another advantage of polymer-based 3D-printed robots is their compatibility with stringent imaging modality requirements, such as the use of magnetic resonance imaging (MRI), especially when intra-operative MRI guidance is required [6]. In this paper, we focus on the discussion of plastic 3D-printing, since metal 3D-printing is relatively expensive and difficult to achieve high accuracy.

Development of 3D-printed surgical robots is currently in its infancy for a variety of reasons. Firstly, there is a lack of large range of materials that can be 3D-printed for use in surgery [7], not to mention the requirements for biocompatibility, sterilizability, and strength

requirements of the robotic system. Secondly, there is a lack of technology to 3D-print sensors and actuators along with the overall robot structure in one build. Given these challenges, the rest of this paper is organized as follows. In Section II, we will review the application of 3D-printing for surgical robotics, as well as the differences between various 3D-printing techniques, biocompatibility, and sterilizability, to name a few. In Section III, we will briefly describe our research in developing 3D-printed surgical robots. In Section IV, we will discuss the challenges and provide our perspectives in developing 3D-printed surgical robots, focusing on 3D-printed actuators and sensors for surgical robots. Finally, some concluding remarks will be made in section V.

II. State of the Art

3D-printing has been extensively used in medical systems, such as prosthetics, anatomical models, surgical guides and templates, implants, etc. A systematic review of 3D-printing in clinical applications shows that the anatomical models for maxillofacial and orthopedic operations are the major medical application of 3D-printing [7]. A 3D-printed anatomical model can help to plan and simulate surgical procedures, construct appropriate surgical tools, and estimate the dimensions of implants [8], [9]. Studies suggest that the pre-operative planning based on 3D-printed anatomical models can decrease the level of risk, number of post-operative complications, and operation time [7]. However, 3D-printed surgical robots have not been reported in any clinical study and only exist in research studies. In this section, we will review the 3D-printing techniques for developing surgical robotic systems and state-of-the-art 3D-printed surgical robots.

A. 3D-Printing Techniques

Fused deposition modeling (FDM), selective laser sintering (SLS), stereolithography apparatus (SLA), and inkjet printing (IJP) are four state-of-the-art 3D-printing technologies that are used in developing surgical robots. In IJP, when multiple print heads are used to print different materials simultaneously, the technique is also referred to as multi-jet printing (MJP). The details of their working principles can be found in the literature [9]. Briefly, SLA uses UV laser to cure photopolymers, SLS uses a high-power laser to fuse small particles of thermoplastic, FDM extrudes small beads of fused thermoplastic materials that are naturally bonded to lower layers, and IJP works by depositing either photocurable plastic resin or casting wax materials layer by layer. To apply 3D-printing for fabricating surgical robots, it is important to satisfy several critical requirements, namely: sterilizability, biocompatibility, smoothness, in addition to other specific material properties for the above-mentioned 3D-printing techniques. 3D-printed materials need to be evaluated in their properties case by case before they can be applied to fabricate surgical robots for specific applications.

1) Sterilizability: To use a 3D-printed surgical robot for clinical applications, the robot must be reliably sterile. Depending on the 3D-printing technique and 3D-printed material, the process of printing itself may be sufficient to sterilize unsterile filament to produce a sterile part. For FDM, the filament is usually extruded at a temperature higher than the temperature required for autoclaving or dry heat sterilization [10]. For example, sterile polylactic acid (PLA) parts were printed by FDM on a building platform that was treated

with ethanol, covered with flame-treated aluminum foil, or placed under a UV lamp [11]. Photopolymerization, used by SLA and some IJP 3D-printers was also found to produce sterile parts [11]. A number of post-printing sterilization options have also been investigated. Autoclaving is the most common sterilization approach in clinics as it can be easily performed, is inexpensive, and non-toxic [12]. The SLA material, PA2200 from EOS (Krailling, Germany), is autoclavable at 134°C. However, the 3D-printed components of a surgical robot must be designed such that all surfaces are directly exposed to the steam [12]. Furthermore, many 3D-printed thermoplastic materials are affected by the autoclaving process. For example, PLA undergoes a decrease in tensile strength and acrylonitrile butadien styrene (ABS) derivatives are physically deformed [13], [14]. An alternative low-temperature solution is gas sterilization. Ethylene oxide (ETO) gas sterilization is simple to operate and works for a significant number of 3D-printed materials (ABS-M30, ABS-M30i, PC-ISO, etc.) [13]. However, since ETO is toxic, it requires 8–12 hours for aeration [12], which can conflict with the requirement of 3D-printing surgical robotic systems quickly for a procedure. Hydrogen peroxide (H_2O_2) gas combines with free radicals to inactivate microorganisms [12] and has worked well for all 3D-printed materials tested by Perez et al. [13]. However, the process was observed to slightly decrease the Young's modulus of PLA and polycarbonate (PC) [15]. Another obstacle for H_2O_2 sterilization is its poor penetration into long, narrow lumens that might arise in the 3D-printed components of a surgical robot, such as a concentric-tube robot [12]. Glutaraldehyde sterilization entails the submersion of 3D-printed components in a glutaraldehyde solution at room temperature for a short period of time. This method is cost-effective and was found not to affect the properties of PLA [16], but the remaining solution within the interiors has to be removed with compressed air [17]. Ionizing radiation, primarily gamma rays, is another low-temperature sterilization technique. It successfully sterilized all 3D-printed materials tested by Perez et al. [13], but the method has deleterious effects on equipment and is not FDA-cleared [12].

2) biocompatibility: Two standards are commonly used to determine the biocompatibility of 3D-printed plastic materials. The U.S. Pharmacopeial Convention (USP) classifies plastics into six classes, among which Class VI is the most stringent [19]. The second standard, IS0–10993 is even more rigorous than the USP Class VI [20]. It is important to note that the FDA approval is still necessary for a surgical robot that is fully printed using a material that has been certified as biocompatible. This study focuses on 3D-printed materials certified by USP Class VI and/or IS0–10993. The off-the-shelf biocompatible materials for the four mainstream 3D-printing techniques are listed in Table I. Although no PLA material for FDM has been certified as biocompatible, an implant made of PLA, polygycolic acid (PGA), and their copolymers was tested *in vivo* and found to be generally biocompatible and non-toxic [21]. Though inflammation was observed 7–20 weeks after implantation due to PLA degradation within organic tissue [21], it should not be an issue if PLA is used to 3D-print a surgical robot that has contact with organic tissue for limited time. Therefore, PLA could be a promising FDM material to satisfy the biocompatibility requirement of surgical robots. So far, no elastomeric 3D-printed material has been certified to be biocompatible. One possible solution is to fabricate a biocompatible sleeve using PDMS [22]. Wang et al. 3D-printed a flexible sleeve to cover a continuum

surgical robot for protection, but the elastomeric material used to 3D-print the sleeve was not biocompatible [23].

3) Smoothness: The smoothness of 3D-printed components is a critical aspect, since it affects the functionality of 3D-printed surgical robots. For example, the components in a tendon-driven surgical robot for tendon routing should be smooth to reduce friction and hysteresis in addition to preventing the tendons from failure due to sharp edges, corners, or surface profile of the channel in which the tendon is routed. The 3D-printed parts can be polished, but fine features may be lost due to polishing, and it is difficult to polish challenging structures, such as small-diameter lumens. Since SLS utilizes laser light to selectively sinter particular areas of powder, support material or structure is not required. However, the surface of a component made by SLS is usually granular and most likely the roughest among the four 3D-printing techniques. Excess powder can be sintered and stuck inside the lumen, which can make the post-processing of the part time consuming. SLA usually produces good surface smoothness, since the liquid photopolymer along the adjacent laser paths is prone to blend together [24]. However, the support material has to be manually removed, so that the macroscopic roughness is high. Since an FDM printer prints a model by depositing melt filament line-by-line, the edges between adjacent lines increase the overall roughness. By using a nozzle of a smaller size (down to 100 μm, Mass Portal, Riga, Latvia), the line thickness and surface roughness can be reduced. IJP can produce the most detailed features due to its fine layer thickness. For example, the layer thickness down to 13 μm can be achieved by the MJP 5600 3D printer (3D Systems, Rock Hill, SC, USA). However, the smoothness of the surface that is planarized by the printer blade is much higher than that of other surfaces. The roughness of a 3D-printed component may be affected by sterilization. For example, the surface may be wrinkled due to chemical reactions when gas sterilization is used [25].

4) Re-usability, Accuracy, Thermal Stability, Stiffness, Uniformity: Since the objective is to develop a patient-specific 3D-printed surgical robot, the robot should be disposable after single use on a patient. Therefore, the re-usability of 3D-printed surgical robots is not critical. 3D-printing accuracy primarily depends on layer thickness (nozzle size for FDM), in addition to post-processing and other factors. Typically, IJP can achieve the smallest layer thickness, followed by SLA, SLS, and FDM. Therefore, IJP can achieve the highest accuracy and the smallest features. The thermal stability of 3D-printed components should be considered for 3D-printed surgical robots that are actuated by thermal shape memory alloys (SMAs). The thermal stability is primarily determined by the glass transition temperature of the 3D-printed material, but the structure also plays an important role. Due to thermal contact conductance, the temperature of the printed components where SMAs are fixed and the adhesive between them, will increase. Therefore, adhesive of higher service temperature and 3D-printed materials of higher glass transition temperature should be used. The design of a 3D-printed component should be optimized to minimize the stress on the area where SMAs are bonded, so that the deformation of the structure at elevated temperature can be minimized. The stiffness of 3D-printed parts is significantly affected by the layer-to-layer adhesion, which is primarily determined by the specific 3D-printing technique and material. Since the stiffness of 3D-printed plastic parts is much smaller than

that of non-3D-printed metallic parts, 3D-printed components should always be designed to minimize the stress and deformation under external loading. The tensile modulus of the biocompatible 3D-printing plastic materials in Table I is in the range of 1 to 4 GPa, while the typical Young's modulus of Aluminum is 69 GPa. As a result, 3D-printed surgical robots may experience positioning error due to the deformation of 3D-printed components [26]. To improve the structural stability of 3D-printed surgical robots, three approaches can be considered. The first approach is to use 3D-printed materials of higher stiffness, such as PEEK and VisiJet M2R-TN listed in Table I, if high 3D-printing accuracy is not required. The second approach is post-curing, which can improve the stiffness of SLA parts by up to 2–3 times by exposing the parts to light of a specific wavelength and at a specific temperature [27]. The third approach is to optimize the design of the surgical robot to minimize the internal stress. For example, a tendon-driven surgical robot should be designed to minimize the probability of approaching the singular configuration, at which point, infinite pulling force is required. Finally, due to the essence of 3D-printing, the uniformity of aforementioned material properties in different directions may be affected by the build direction. For example, the stiffness is highest in the build direction for SLA printed specimens [28].

B. 3D-Printed Surgical Robots

According to the fabrication procedures, 3D-printed surgical robots can be divided into two categories, namely: semi and fully 3D-printed surgical robots. The reason for such classification is to distinguish between the surgical robots that are completely 3D-printed and the surgical robots that are assembled from 3D-printed and non-3D-printed components. A fully 3D-printed robot may be assembled from components that are individually 3D-printed. However, a monolithic, fully 3D-printed surgical robot, could be the long-term objective if all the actuation/transmission and sensing components can be 3D-printed in a cost-efficient manner. All 3D-printed surgical robots reported in the literature are semi 3D-printed robots. This is primarily due to the fact that a fully functional surgical robotic system consists of many subsystems, such as actuation, transmission, sensing, and the robot body, and only some subsystems or parts of subsystems can be 3D-printed.

The transmission system is directly driven by actuators and it interfaces with the robot body. MRI-safe, disposability, and compactness are the three primary benefits of 3D-printed transmission. A 3D-printed plastic transmission system can manipulate a non-magnetic tool so that the surgical robot can perform procedures under MRI guidance [29]–[31]. By developing a 3D-printed transmission system, the surgical robot is disposable due to the relatively low cost of 3D-printing and furthermore there is also no maintenance cost. For example, a single-use transmission system with three degrees-of-freedom (DoFs) and essential compliance was 3D-printed for ENT (ear, nose, and throat) surgery [18]. Due to the design freedom associated with 3D-printing, complex waffle gears were 3D-printed to develop a compact transmission system for a concentric-tube robot [32]. The only 3D-printed actuation system for surgical robots that is reported in the literature is a pneumatic actuation mechanism, where a multi-DoF actuation mechanism is 3D-printed as a monolithic component, so that the system is compact and laborious assembly can be avoided [30].

A surgical robot usually possesses a slender and meso-scale footprint that can be actively reconfigured. According to their kinematics, surgical robots can be classified into two main categories: soft, continuum robots versus rigid, articulated robots. As a typical example of the first category, a 3D-printed concentric-tube robot is assembled from 3D-printed plastic tubes driven by remote non-3D-printed actuators [24], [33]. Since the pre-curved configurations of plastic tubes can be easily programmed during 3D-printing, complicated thermal training procedures required by conventional concentric-tube robots made of superelastic nitinol tubes are not required. Therefore, a patient-specific concentric-tube robot can be fabricated efficiently [32]. In the first category, semi-3D-printed continuum surgical robots for neurosurgical applications have also been developed by actuating local joints using shape memory alloy (SMA) actuators [34] or actuating spring backbone using tendons [35]. In the second category, non-3D-printed rigid actuators are embedded within 3D-printed structures to form an articulated manipulator. For example, brushless DC motors were encased inside 3D-printed casings to actuate a reconfigurable robot for endoluminal interventions [26].

III. Main Accomplishments

This section will present the main accomplishments in our group in developing 3D-printed surgical robots for the following three projects: Minimally Invasive Neurosurgical Intracranial Robot (MINIR-II), Neurosurgical Intracerebral Hemorrhage Evacuation (NICHE) robot, and a robotic catheter for atrial fibrillation (AFib) treatment. Due to the relatively low cost, short fabrication period, and capability of fabricating complicated structures with the high accuracy of 3D-printing, the design of the developed surgical robots can potentially be customized for specific surgical procedures to achieve improved surgical outcomes, such as enhanced tumor removal rate and reduced trauma. Due to the low glass transition temperatures of 3D-printed materials used in these projects, low-temperature sterilization methods, such as gas sterilization and Glutaraldehyde sterilization, may be applicable, but investigation is required to evaluate the influence of these processes on the properties of 3D-printed parts.

A. MINIR-II

Brain tumor is one of the most common cancers and the most common causes of cancer-related death among children and young adults [36]. Its impact on the quality of life of brain cancer patients is undisputed. The MINIR-II robot is a tendon-driven continuum robot developed for brain tumor removal under MR imaging guidance [35], [37]. As shown in Fig. 1, the MINIR-II robot consists of a three-segment spring backbone with an outer diameter of 4.2 mm. Two pairs of monofilament wires are routed at each segment along its central axis to achieve independent segment motion. The cables are kept at reasonable tension to cancel out the effect of gravity on the spring and alleviate backlash. A soft sleeve was 3D-printed in the elastomeric CE-NT material (VisiJet®, 3D Systems) at a layer thickness of 13 μm using the MJP 5600 3D printer and threaded through the robot for protection.

To 3D print the spring backbone as a monolithic piece and ensure that each segment can bend by at least 90°, we have explored several 3D-printing techniques and different

combinations of spring dimensions. It is challenging to 3D print a plastic spring at such a small scale due to the normally aggressive post-processing steps involved to remove the support material, such as immersion in corrosive liquid, water jetting, and manual support structure breaking and scraping. The spring backbone was 3D-printed in VeroWhite material on an Objet 350V 3D printer (Stratasys, Eden Prairie, MN, USA), and the support material was manually scraped with extreme care using dental probes. However, the success rate was only about 20%. This is contradictory to the fundamental concept of 3D-printing, which is to allow fast prototyping for patient-specific surgical robots. An alternative solution was to use three individual SMA springs as the backbone [38]. The stiffness of each SMA spring can be actively adjusted by controlling its temperature using Joule heating due to the phase transformation of SMA. The SMA springs were connected in series and electrically insulated by threading each end of the spring onto the screw connector on each side of a 3D-printed segment disk. Recently, we have succeeded in 3D-printing a monolithic plastic spring backbone with a clean lumen and coil space without any damage in the CR-CL material (VisiJet®, 3D Systems) at a layer thickness of 13 μm on the MJP 5600 3D printer due to the decent post-processing procedures. Wax support material can be easily removed by placing the 3D-printed component in an oven at 65 °C followed by ultrasonic cleaning at 60 °C. In this process, no mechanical force is applied. However, at elevated temperature, the gap between adjacent spring turns becomes nearly zero due to the release of internal strain and the spring backbone may be deformed due to gravity. It was also observed that the spring backbone became more brittle (easier to break during bending or with less bending cycles) after around three months of being under constant compression due to the cable tension. This is consistent with a previous report about degradation of mechanical properties of polyjet/multijet-printed materials [39]. However, this is not a significant concern since the robot is designed to be patient-specific and disposed after single use.

To isolate the disposable MINIR-II robot with the reusable actuation/transmission system for the simplicity of sterilization, a quick-connect module was developed based on the concept of gear matching and snap fitting [23]. The quick-connect module consists of a proximal housing that leads to the actuation system and a distal housing that leads to the robot. These two housings can be connected together using a clip on the top and a carriage on the bottom. There are two sets of six gears (responsible for six DoFs of the robot) in each housing of the quick-connect module. Each gear is customized to route cables in a thin circular slot and to prevent tangling of the cables with the gear teeth. All the aforementioned parts were 3D-printed in CR-CL, which provides sufficient strength (tensile modulus of up to 2.1 GPa, as shown in Table I) and durability (impact strength of 21–30 J/m). It should be noted that dimension selection is also important, especially for parts subject to any external load, to resist potential deformation.

The actuation/transmission system was designed to provide a stable, accurate, and efficient control of the MINIR-II robot, as shown in Fig. 2(a). Ultrasonic motors are used for actuation due to the requirement of MRI-safe. To minimize the electric noise on MRI, a switching mechanism was developed to actuate the 6-DoF robot by using three ultrasonic motors, as shown in Fig. 2(b). To realize a lightweight system, fabricate complex components, and ensure it is MRI-safe, the majority of the actuation/transmission system was 3D-printed in CR-CL. However, high aspect-ratio components are likely to be deformed

by gravity during post-processing, resulting in the decrease in dimensional accuracy. Deformation was also observed in some of the 3D-printed plastic components that are subject to high external loading conditions. To address this issue, more flexibility was designed at the mating locations or surfaces. For example, since the 3D-printed unit that would be moved by cams was not accurate enough, the position of the two cam followers on that unit was designed to be adjustable after assembly. For critical components that experience high stress, such as long transmission shafts and screws, non-magnetic metals or molded plastics were used. Friction is another critical issue. Since the mating surfaces of 3D-printed cams and gears were not smooth enough, fine sand papers were used to polish them. For gears with teeth in a narrow space, a gear with complex features was 3D-printed and combined with an off-the-shelf molded plastic gear for force transmission.

Due to the design freedom involved in 3D-printing, the MINIR-II robot can be readily modified to be integrated with a bending sensor module. The sensor module is developed by connecting a 1 mm diameter superelastic spring in series with a Polydimethylsiloxane (PDMS) cylinder with an embedded 190 μm diameter fiber Bragg grating (FBG) fiber. Since each robot segment consists of a spring between two disks, the sensor module is integrated with the robot segment by bonding its two ends onto the two disks. Therefore, when the robot segment is deflected, the sensor module will be elongated, which results in normal strain in the FBG fiber and wavelength shift of the reflected light. Due to the low bending stiffness of the FBG-PDMS assembly, the sensor module has negligible influence on the flexibility of the MINIR-II robot. Due to the reinforcement effect by the FBG fiber, the FBG-PDMS assembly has a high axial stiffness and the primary elongation occurs on the spring. The FBG-PDMS assembly is fabricated by curing the PDMS solution in Teflon tubing within which the FBG fiber is pre-placed and gluing the superelastic spring to the PDMS cylinder using super glue. We have successfully measured bending deflection of the MINIR-II robot up to 30°, but hysteresis has been observed.

The working performance of the MINIR-II robot was evaluated under MR imaging guidance. The earliest prototype of the MINIR-II robot, which was actuated by cooling module-integrated SMA spring actuators, was tested in a 3 T Siemens MR scanner using a gelatin phantom [37], [40]–[42]. The mean signal-to-noise ratio (SNR) dropped by 6.4% upon robot actuation. The MINIR-II robot with the aforementioned actuation/transmission system was tested in the same MR scanner using a human cadaver head. As shown in Fig. 3, the capability of the robot in moving inside the brain tissue was confirmed. There was less than 2% SNR change every time the robot changed its status. Therefore, the entire MINIR-II robotic system is MRI-safe.

B. NICHE

Spontaneous intracerebral hemorrhage (ICH) occurs in about 2 million people worldwide every year [43]. The NICHE robot was developed for ICH evacuation to immediately alleviate the pressure applied on brain tissue and stop further damage to critical brain functions [34], [44]. The robot tip is required to have a large workspace to remove a significant volume of ICH with negligible disruption to healthy brain tissue. Therefore, the NICHE robot is designed to consist of a torsion actuator and a distal bending tip to realize

tip articulation, in addition to a rigid and hollow stem. Electrocautery probes and suction tubing are equipped to soften and evacuate blood clot. Most of the structural components are 3D-printed in CR-CL. The torsion actuator can be bi-directionally actuated by two pre-deformed antagonistic SMA torsion springs [45], [46]. A rotary disk and a shaft are 3D-printed as a monolithic piece and supported by micro bearings inside the actuator housing. One end of each spring is bonded to the rotary disk and the other to the actuator housing. By individually heating each SMA torsion spring via Joule heating, the spring will recover its memorized configuration and the shaft will be rotated. Surgical accessories and wires can pass through the lumen of the shaft. To minimize the diameter of the shaft for large deformation of springs and large motion range, the thickness of the wall of the shaft is only 0.5 mm. Due to the internal stress and increased temperature of the rotary disk/shaft upon SMA actuation, the CR-BK material (VisiJet®, 3D Systems) is used to print the rotary disk/shaft at a layer thickness of 13 μm using the MJP 5600 3D printer because of its higher stiffness and glass transition temperature than CR-CL. The rotary disk/shaft is printed horizontally with its axis 45° offset from the planarization direction to enhance its torsional rigidity. The actuator housing has a small thickness of 0.3 mm to maximize the inner space that accommodates the SMA springs. The bending tip can be bi-directionally actuated by a pair of antagonistic SMA wires, which recover opposite curved configurations at high temperature. Backbone disks are threaded through the SMA wires to minimize the twisting motion of the bending tip. The backbone disks have a thickness of 0.6 mm and are printed in CR-BK. The overall weight of the NICHE robot is about 4.3 g.

A skull-mounted robotic headframe was also developed to manipulate the NICHE robot and to align it with a predefined trajectory [47], as shown in Fig. 5(a). The headframe is comprised of a pedestal, a Stewart platform, and a linear actuation module. Most of the structural components are printed in Clear resin on a Form 2 3D printer (Formlabs, Somerville, MA, USA) or CR-CL to realize a lightweight headframe. In the Stewart platform, the upper and lower plates are connected by six linear actuators via universal and ball joints. The pedestal can be fixed on the skull using brass screws and the lower plate of the Stewart platform can be mounted onto the pedestal using plastic screws. The linear actuation module consists of a base plate, a linear bearing inside a housing, a hollow gear rack, and a pinion that couples the gear rack with the motor shaft, as shown in Fig. 5(b). The NICHE robot can be connected to the lower end of the gear rack via a snap-fit mechanism, as shown in Fig. 5(c). Thus, the NICHE robot can be translated by the DC motor. Due to the rigidity and stability of parallel robots, the headframe can achieve about 1 mm positioning accuracy at the robot tip in 3D-space, even if the stiffness of plastic 3D-printed material is not very high.

A rotation sensor was developed based on fiberoptic light intensity modulation [48], [49]. All the structural components were 3D-printed in CR-CL. By mounting the sensor rotor on the shaft of the SMA torsion actuator, the motion of the actuator can be measured and feedback controlled. As shown in Fig. 4(c), the sensor rotor is supported by a micro bearing. A reflector, i.e. a polished brass disk, is placed on the slanted side of the sensor rotor. Several sets of optical fibers are installed in the sensor housing. Therefore, when the sensor rotor is rotated by the actuator, the intensity of the light received by the optical fibers is reflected by the brass reflector. The system modeling shows that the sensitivity can be more

consistent by using more sets of optical fibers. As shown in Fig. 4(d), the NICHE robot is capable of performing precise tip articulation when the torsion actuator is feedback controlled. The NICHE robot equipped with the fiberoptic rotation sensor was evaluated using a human cadaver head under computed tomography (CT) imaging guidance, as shown in Fig. 6(a). Fig. 6(b) shows that artifacts are induced by metallic bearings and screws in the CT image, while the area around the fully 3D-printed end-effector is not affected. Afterwards, the NICHE robot without the fiberoptic rotation sensor was evaluated under MR imaging guidance, as shown in Fig. 6(c). As shown in Fig. 6(d), the deflected robot tip can be clearly identified in relationship to soft-tissue brain structures.

C. Robotic Catheter for AFib

AFib is an irregular heartbeat caused by abnormal electric signals from pulmonary veins in the left atrium. To treat AFib, a catheter can be used to ablate heart tissue and block abnormal electric signals. Due to the low accessibility of ablation targets, we have developed a robotic catheter with a steerable tip [50]. Since MR imaging can be used to evaluate the formation of fibrosis, which is an indicator of the success in ablation, SMA actuators under conductive heating were utilized. As shown in Fig. 7(a), the robotic catheter consists of flexible braid-reinforced tubing and a steerable tip comprised of multiple bending modules. Each bending module is bi-directionally actuated by a pair of antagonistic SMA wires that are bonded between two rigid links 3D-printed in CR-CL. Two bending modules are assembled together via the recess and extrusion on the links. To realize conductive heating actuation, nichrome coils are routed around each SMA wire by following a spiral path of a 3D-printed jig, as shown in Fig. 7(b). Due to the small diameter and high resistivity of nichrome wires, very low electric current (less than 100 mA) is required to actuate the bending module, so that the electromagnetic noise on MR imaging is negligible. As shown in Fig. 7(c), the catheter tip was actuated in water, and the quality of MR imaging was consistent regardless of SMA actuation.

The 3D-printed rigid links of the SMA bending module can be easily modified to accommodate a customized bending sensor. The sensor is developed by bonding the grating segment of an FBG fiber on each of the two sides of a 800 μm wide and 76.2 μm thick superelastic nitinol substrate. To fabricate the sensor, the substrate and FBG fibers are aligned using a jig, followed by applying flexible UV-cured glue and shining UV light. The jig was 3D-printed in CR-CL on the MJP 5600 3D printer due to its capability in printing small and complex structures to accommodate the FBG fibers and substrate. When the sensor is deflected, normal strain in FBG fibers is induced due to the shear stress in the flexible adhesive, resulting in the wavelength shift of the reflected light. The sensor is integrated with the bending module by gluing one end of the sensor in the slot of the rigid link, while the other end slides in the slot of the other link. However, due to the friction applied by the rough slot of the 3D-printed link, hysteresis was observed in the sensor output.

IV. CHALLENGES AND PERSPECTIVES

A. 3D-Printed Materials

To satisfy the requirements of surgical applications, any exposed surface area on 3D-printed parts should be sterilizable and biocompatible, properties which have been achieved by some 3D-printed materials. Additionally, thermal stability is required by SMA actuated surgical robots, but a high glass transition temperature is challenging to achieve in plastic 3D-printed materials without sacrificing 3D-printing accuracy.

The literature shows that the primary application of 3D-printing in surgical robots is to fabricate structural components. Since these structures may have different rigidity requirements, a wide range of stiffness options, from elastomeric to metal-like, is preferred in 3D-printed materials. However, finding 3D-printed materials on either end of this range that are suitable for surgical robots, is a challenge. No elastomeric 3D-printed material found was reported to meet the highest level of biocompatibility standards, and increasing the stiffness of the more rigid 3D-printed materials is difficult while maintaining low density. Small features are required to create compact surgical robots that minimize the invasiveness of interventional procedures, but these small-feature structures (i.e. thin walls) usually have low rigidity and cannot sustain high loading due to the relatively low stiffness of plastic 3D-printed materials.

Durability may also pose a challenge as many 3D-printed materials tend to degrade over time in different ways, causing a powdery and rough surface finish, shape and structure deformation, or surface yellowing. However, this would not be a concern for single-use, patient-specific, surgical robots. 3D-printed support material and associated post-processing techniques are almost as important as the 3D-printed material to successfully fabricate surgical robots with ideal properties. Post-processing approaches that can thoroughly remove support material without changing the mechanical and geometric properties of 3D-printed components are in high demand.

B. Semi 3D-Printed Surgical Robots

Semi 3D-printed surgical robots are the mainstream of current 3D-printed surgical robots and probably will remain so in the near future. The primary challenge for semi 3D-printed surgical robots is the laborious work of assembling 3D-printed structures with non-3D-printed components, such as actuators and sensors. For example, the tendon wires have to be manually tied onto the 3D-printed spring backbone of the MINIR-II robot [37]. To simplify the fabrication of semi 3D-printed surgical robots, application-based 3D-printing was proposed [51].

For application-based 3D-printing, 3D models are designed with cavities to accommodate the components that are manually assembled after printing in traditional 3D-printing. In application-based 3D-printing, the building process will be paused at a specific time, so that non-3D-printed components can be embedded to the build and then the building process will be resumed. For example, tendon wires can be embedded in the middle of 3D-printing a tendon-driven surgical robot, so that the tedious work of routing tendon wires can be alleviated. Other potential non-3D-printed components for application-based 3D-printing

may include, but are not limited to, FBG fibers, OCT cameras, scissors, etc. A shape converter may be pre-printed to hold the non-3D-printed components of tricky geometry and embedded as an assembly [51].

There are three considerations in designing application-based 3D-printing procedures. Firstly, if the embedded components need to be fixed, adhesive may be applied or 3D-printed fixtures can be designed. Secondly, the embedded components and embedding process should not interfere with subsequent printing. Finally, the 3D model of the component should be optimally placed in the software to facilitate the embedding process, since the model is 3D-printed layer by layer. Therefore, it is challenging to apply this technique in SLA printers, since the building platform is immersed in the liquid resin, or the model is printed up-side down. This technique may be feasible for FDM and SLS, since they do not require support material and the building platforms can be easily accessed. To apply this technique in IJP, support material need to be removed with care and the embedded structure has to be flush with the printed volume to avoid collision with print heads.

C. Fully 3D-Printed Surgical Robots

Fully 3D-printed surgical robots is necessary to realize the full potential of 3D-printed surgical robots, since most of the laborious assembly work of putting together various 3D-printed subcomponents along with various sensors and actuators, cannot be understated. Technicians can develop the surgical robots for specific patients by modifying all the structural components, actuators, and sensors on the computer-aided design (CAD) software before sending the model for printing. To develop a functional fully 3D-printed surgical robot, 3D-printed actuators and sensors need to be explored. However, 3D-printed actuators and sensors are at a very early stage of development and none of them have been applied in surgical robots.

Considering the required stimulus, stroke, force, and motion forms, shape memory polymer (SMP), electroactive polymer (EAP), and fluid driven actuators are the three most promising types for fully 3D-printed surgical robots. The release of internal strain is one of primary principles for SMP and it takes place at temperature higher than its glass transition (GT) temperature [58]. So far, MJP, SLA, and FDM have been reported in 3D-printing unidirectional SMP, as listed in Table II. Since MJP can blend different SMP materials and print different materials in one batch, GT temperature can be adjusted [56] and a monolithic SMP actuator of different GT temperatures at different locations can be printed [59]. SLA can also adjust GT temperature by adjusting the constituents and composition of resins and the highest recoverable strain is achieved by SLA [55]. However, two-way shape memory effect (SME), which is necessary to actuate a surgical robot, has not been reported in this type of SMP. Two-way SME can be realized in SMP composites via the difference in hydraulic swelling ratio [60]–[62] or thermal expansion (CTE) [63]. Ionic polymer-metal composite (IPMC) morphologically transforms under an electric field due to the movement of cations and solvent molecules. A bucky gel IPMC actuator, which was developed by printing electrode and electrolyte in carbon nanotubes, ionic liquids, and polymers, was able to work in a dry environment [64]. Dielectric elastomer (DE) is another type of EAP actuator that can be 3D-printed in silicone dielectric elastomer, but extremely high excitation

voltage makes it inappropriate for surgical applications [65]. Compared with EAP, stimulus for fluid driven actuators are more friendly to the surgical environment. Since the stretchability of most 3D-printed plastics is much lower than that of silicone-based elastomers that are usually used to fabricated fluid driven actuators, bellow or diaphragm structure is employed in 3D-printed pneumatic actuators [66], [67]. By using highly stretchable elastomeric 3D-printed materials, more freedom will be obtained in designing compact 3D-printed actuators for surgical robots. However, no elastomeric 3D-printing material has been certified to be biocompatible.

Force and shape sensing systems are crucial to the success of surgical procedures performed by surgical robots. A force sensor can monitor the force applied on soft tissue to ensure it is appropriate and a shape sensor can measure the robot configuration in real-time for feedback control of the robot configuration. 3D-printing has been widely applied in developing sensors for many different medical applications [68], [69]. In terms of shape sensing, a stretchable strain sensor was developed by 3D-printing conductive ink into an uncured elastomeric reservoir [70]. This sensor was demonstrated on a glove, but can be potentially used as a shape sensing sleeve, since the non-biocompatible ink was embedded in the elastomer matrix. In terms of force sensing, a semi 3D-printed force sensor can be developed by combining metal flexures with metallic or fiberoptic transducers in a 3D-printed structure [71]. It is possible to completely 3D-print force sensors by printing conductive elastomer [72]. When a force is applied, the printed structure can be deformed and the resistance will be changed [72].

V. Conclusions

To develop patient-specific surgical robots, 3D-printing technology will require several more advances, as discussed in this paper. 3D-printed surgical robots are currently at a very early stage of development. One of the root causes is the extremely stringent requirements of 3D-printed materials, including but not limited to, sterilizability, biocompatibility, surface smoothness, thermal stability, and stiffness. In this paper, we have reviewed the state-of-the-art in developing 3D-printed surgical robots and also presented our accomplishments in applying 3D-printing techniques to develop neurosurgical and cardiovascular surgical robots. The majority of current 3D-printed surgical robots are semi 3D-printed and hence require manually combining 3D-printed structures with non-3D-printed actuators, sensors, or transmission mechanisms. We have discussed application-based 3D-printing to facilitate semi 3D-printed surgical robots. To completely 3D print surgical robots, 3D-printed actuators and sensors need further investigations, in addition to appropriate design of surgical robots. Most 3D-printed sensors and actuators are currently semi 3D-printed and do not come close to satisfying the stringent requirements for surgical robots. In conclusion, 3D-printing technology is still in its infancy and will require significantly more research for the development of patient-specific 3D-printed surgical robots.

ACKNOWLEDGMENT

References

[1]. Kwoh YS, Hou J, Jonckheere E, Hayati S, et al., "A robot with improved absolute positioning accuracy for CT guided stereotactic brain surgery," Biomedical Engineering, IEEE Transactions on, vol. 35, no. 2, pp. 153–160, 1988.

[2]. Moskowitz RM, Young JL, Box GN, Paré LS, and Clayman RV, "Retroperitoneal transdiaphragmatic robotic-assisted laparoscopic resection of a left thoracolumbar neurofibroma," JSLS, Journal of the Society of Laparoendoscopic Surgeons, vol. 13, no. 1, pp. 64–68, 2009. [PubMed: 19366544]

[3]. Vaidya A, "11 things to know about robotic surgery," 7 2015 [Online]. Available: https://www.beckersasc.com/asc-turnarounds-ideas-to-improve-performance/11-things-to-know-about-robotic-surgery.html

[4]. Tighe PJ, Badiyan S, Luria I, Boezaart AP, and Parekattil S, "Robot-assisted regional anesthesia: a simulated demonstration," Anesthesia and Analgesia, vol. 111, no. 3, p. 813, 2010. [PubMed: 20581161]

[5]. Morimoto TK, Greer JD, Hawkes EW, Hsieh MH, and Okamura AM, "Toward the design of personalized continuum surgical robots," Annals of Biomedical Engineering, pp. 1–12, 2018.

[6]. Kim Y, Cheng SS, Diakite M, Gullapalli RP, Simard JM, and Desai JP, "Toward the development of a flexible mesoscale MRI-compatible neurosurgical continuum robot," IEEE Transactions on Robotics, vol. 33, no. 6, pp. 1386–1397, 2017. [PubMed: 29225557]

[7]. Martelli N, Serrano C, van den Brink H, Pineau J, Prognon P, Borget I, and El Batti S, "Advantages and disadvantages of 3-dimensional printing in surgery: a systematic review," Surgery, vol. 159, no. 6, pp. 1485–1500, 2016. [PubMed: 26832986]

[8]. Malik HH, Darwood AR, Shaunak S, Kulatilake P, Abdulrahman A, Mulki O, and Baskaradas A, "Three-dimensional printing in surgery: a review of current surgical applications," Journal of Surgical Research, vol. 199, no. 2, pp. 512–522, 2015. [PubMed: 26255224]

[9]. Rengier F, Mehndiratta A, Von Tengg-Kobligk H, Zechmann CM, Unterhinninghofen R, Kauczor H-U, and Giesel FL, "3D printing based on imaging data: Review of medical applications," International Journal of Computer Assisted Radiology and Surgery, vol. 5, no. 4, pp. 335–341, 2010. [PubMed: 20467825]

[10]. Fedorovich NE, Alblas J, Hennink WE, Öner FC, and Dhert WJ, "Organ printing: the future of bone regeneration?" Trends in Biotechnology, vol. 29, no. 12, pp. 601–606, 2011. [PubMed: 21831463]

[11]. Neches RY, Flynn KJ, Zaman L, Tung E, and Pudlo N, "On the intrinsic sterility of 3D printing," PeerJ, vol. 4, p. e2661, 2016.

[12]. "Infection control," 9 2016 [Online]. Available: https://www.cdc.gov/infectioncontrol/guidelines/disinfection/sterilization/index.html

[13]. Perez M, Block M, Espalin D, Winker R, Hoppe T, Medina F, and Wicker R, "Sterilization of FDM-manufactured parts," in Proceedings of the 2012 Annual International Solid Freeform Fabrication Symposium, Austin, TX, 8, 2012, pp. 6–8.

[14]. Rozema F, Bos R, Boering G, Van Asten J, Nijenhuis A, and Pennings A, "The effects of different steam-sterilization programs on material properties of poly (l-lactide)," Journal of Applied Biomaterials, vol. 2, no. 1, pp. 23–28, 1991. [PubMed: 10150042]

[15]. Sosnowski E and Morrison J, "Sterilization of medical 3D printed plastics: Is H2O2 vapour suitable?" CMBES Proceedings, vol. 40, no. 1, 5 2017 [Online]. Available: https://proceedings.cmbes.ca/index.php/proceedings/article/view/622

[16]. Rankin TM, Giovinco NA, Cucher DJ, Watts G, Hurwitz B, and Armstrong DG, "Three-dimensional printing surgical instruments: Are we there yet?" Journal of Surgical Research, vol. 189, no. 2, pp. 193–197, 2014. [PubMed: 24721602]

[17]. Safety O, Administration H, et al., "Best practices for the safe use of glutaraldehyde in health care," US Department of Labor, 2006.

[18]. Entsfellner K, Kuru I, Maier T, Gumprecht JD, and Lueth TC, "First 3D printed medical robot for ENT surgery-Application specific manufacturing of laser sintered disposable manipulators," in Intelligent Robots and Systems (IROS 2014), 2014 IEEE/RSJ International Conference on. IEEE, 2014, pp. 4278–4283.

[19]. "What is USP class vI testing and why is it important," 10 2013 [Online]. Available: https://hollandaptblog.com/2013/10/14/what-is-usp-class-vi-testing-and-why-is-it-important/

[20]. "What is ISO 10993? How is it different from USP class VI?" 4 2014 [Online]. Available: https://hollandaptblog.com/2014/04/22/what-is-iso-10993-how-is-it-different-from-usp-class-vi/

[21]. Athanasiou KA, Niederauer GG, and Agrawal CM, "Sterilization, toxicity, biocompatibility and clinical applications of polylactic acid/polyglycolic acid copolymers," Biomaterials, vol. 17, no. 2, pp. 93–102, 1996. [PubMed: 8624401]

[22]. Bae WJ, Kim KS, Kim SJ, Cho HJ, Hong SH, Lee JY, Hwang T-K, and Kim SW, "AB222. comparison of biocompatibility between PDMS and PMMA as packaging materials for the intravesical implantable device: changes of macrophage and macrophage migratory inhibitory factor," Translational Andrology and Urology, vol. 3, no. Suppl 1, 2014.

[23]. Wang X, Cheng SS, and Desai JP, "Design, analysis, and evaluation of a remotely-actuated MRI-compatible neurosurgical robot," IEEE Robotics and Automation Letters, 2018.

[24]. Morimoto TK and Okamura AM, "Design of 3-D printed concentric tube robots." IEEE Transactions on Robotics, vol. 32, no. 6, pp. 1419–1430, 2016. [PubMed: 28713227]

[25]. Lee MH, Kim H-L, Kim CH, Lee SH, Kim JK, Lee SJ, and Park J-C, "Effects of low temperature hydrogen peroxide gas on sterilization and cytocompatibility of porous poly (D, L-lactic-coglycolic acid) scaffolds," Surface and Coatings Technology, vol. 202, no. 22–23, pp. 5762–5767, 2008.

[26]. Harada K, Susilo E, Menciassi A, and Dario P, "Wireless reconfigurable modules for robotic endoluminal surgery," in Robotics and Automation, 2009. ICRA'09. IEEE International Conference on. IEEE, 2009, pp. 2699–2704.

[27]. "Form 2 tech specs." [Online]. Available: https://formlabs.com/3d-printers/form-2/tech-specs/

[28]. Alharbi N, Osman R, and Wismeijer D, "Effects of build direction on the mechanical properties of 3d-printed complete coverage interim dental restorations," The Journal of prosthetic dentistry, vol. 115, no. 6, pp. 760–767, 2016. [PubMed: 26803175]

[29]. Li G, Su H, Cole GA, Shang W, Harrington K, Camilo A, Pilitsis JG, and Fischer GS, "Robotic system for MRI-guided stereotactic neurosurgery," IEEE Transactions on Bio-medical Engineering, vol. 62, no. 4, p. 1077, 2015. [PubMed: 25376035]

[30]. Comber DB, Slightam JE, Gervasi VR, Neimat JS, and Barth EJ, "Design, additive manufacture, and control of a pneumatic MR-compatible needle driver," IEEE Transactions on Robotics, vol. 32, no. 1, pp. 138–149, 2016. [PubMed: 31105476]

[31]. Guo Z, Dong Z, Lee K-H, Cheung CL, Fu H-C, Ho JD, He H, Poon W-S, Chan DT-M, and Kwok K-W, "Compact design of a hydraulic driving robot for intra-operative MRI-guided bilateral stereotactic neurosurgery," IEEE Robotics and Automation Letters, vol. 3, no. 3, pp. 2515–2522, 2018.

[32]. Morimoto TK, Hawkes EW, and Okamura AM, "Design of a compact actuation and control system for flexible medical robots." IEEE Robotics and Automation Letters, vol. 2, no. 3, pp. 1579–1585, 2017. [PubMed: 28664187]

[33]. Amanov E, Nguyen T-D, and Burgner-Kahrs J, "Additive manufacturing of patient-specific tubular continuum manipulators," in Medical Imaging 2015: Image-Guided Procedures, Robotic Interventions, and Modeling, vol. 9415. International Society for Optics and Photonics, 2015, p. 94151P.

[34]. Sheng J and Desai JP, "Towards a SMA-actuated neurosurgical intracerebral hemorrhage evacuation (NICHE) robot," in Intelligent Robots and Systems (IROS), 2015 IEEE/RSJ International Conference on. IEEE, 2015, pp. 3805–3810.

[35]. Kim Y, Cheng SS, and Desai JP, "Towards the development of a flexible meso-scale MRI-compatible neurosurgical continuum robot," IEEE Transactions on Robotics, 2017.

[36]. Facts & figures 2018: Rate of deaths from cancer continues decline. Available: https://www.cancer.org/latest-news/facts-and-figures-2018-rate-of-deaths-from-cancer-continues-decline.html.

[37]. Cheng SS, Kim Y, and Desai JP, "New actuation mechanism for actively cooled SMA springs in a neurosurgical robot," IEEE Transactions on Robotics, 2017.

[38]. Kim Y, Cheng SS, and Desai JP, "Active stiffness tuning of a spring-based continuum robot for MRI-guided neurosurgery," IEEE Transactions on Robotics, vol. 34, no. 1, pp. 18–28, 2018. [PubMed: 29434530]

[39]. Dizon JRC, Espera AH Jr, Chen Q, and Advincula RC, "Mechanical characterization of 3d-printed polymers," Additive Manufacturing, vol. 20, pp. 44–67, 2018.

[40]. Cheng SS and Desai JP, "Towards high frequency actuation of SMA spring for the neurosurgical robot-MINIR-II," in Robotics and Automation (ICRA), 2015 IEEE International Conference on. IEEE, 2015, pp. 2580–2585.

[41]. Cheng SS, Kim Y, and Desai JP, "Modeling and characterization of shape memory alloy springs with water cooling strategy in a neuro-surgical robot," Journal of Intelligent Material Systems and Structures, p. 1045389X16685443, 2017.

[42]. Cheng S, Kim Y, and Desai JP, "Towards real-time SMA control for a neurosurgical robot: MINIR-II," in Robotics Research. Springer, 2018, pp. 187–200.

[43]. Qureshi AI, Mendelow AD, and Hanley DF, "Intracerebral haemorrhage," The Lancet, vol. 373, no. 9675, pp. 1632–1644, 2009.

[44]. Sheng J, Gandhi D, Gullapalli RP, Simard JM, and Desai JP, "Development of a meso-scale SMA-based torsion actuator for image-guided procedures." IEEE Transactions on Robotics, vol. 33, no. 1, pp. 240–248, 2017. [PubMed: 28210189]

[45]. Sheng J and Desai JP, "Design, modeling and characterization of a novel meso-scale SMa-actuated torsion actuator," Smart Materials and Structures, vol. 24, no. 10, p. 105005, 2015.

[46]. Sheng J and Desai JP, "A novel meso-scale SMA-actuated torsion actuator," in Intelligent Robots and Systems (IROS), 2015 IEEE/RSJ International Conference on. IEEE, 2015, pp. 4718–4723.

[47]. Sheng J and Desai JP, "A skull-mounted robotic headframe for a neurosurgical robot," in Intelligent Robots and Systems (IROS), 2017 IEEE/RSJ International Conference on. IEEE, 2017, pp. 2511–2516.

[48]. Sheng J and Desai JP, "Development of a mesoscale fiberoptic rotation sensor for a torsion actuator," IEEE Robotics and Automation Letters, vol. 3, no. 1, pp. 537–543, 2018. [PubMed: 29503870]

[49]. Sheng J and Desai JP, "A highly compact fiberoptic rotation sensor for a neurosurgical robot," in Medical Robotics (ISMR), 2018 International Symposium on. IEEE, 2018, pp. 1–6.

[50]. development of a steerable and MRI-compatible cardiac catheter for atrial fibrillation treatment," IEEE Robotics and Automation Letters, vol. 3, no. 4, pp. 4038–4045, 2018. [PubMed: 30923746]

[51]. Meisel NA, Elliott AM, and Williams CB, "A procedure for creating actuated joints via embedding shape memory alloys in PolyJet 3D printing," Journal of Intelligent Material Systems and Structures, vol. 26, no. 12, pp. 1498–1512, 2015.

[52]. Zhang Q, Yan D, Zhang K, and Hu G, "Pattern transformation of heat-shrinkable polymer by three-dimensional (3D) printing technique," Scientific Reports, vol. 5, p. 8936, 2015. [PubMed: 25757881]

[53]. Zhou Y, Huang WM, Kang SF, Wu XL, Lu HB, Fu J, and Cui H, "From 3D to 4D printing: Approaches and typical applications," Journal of Mechanical Science and Technology, vol. 29, no. 10, pp. 4281–4288, 2015.

[54]. Yang Y, Chen Y, Wei Y, and Li Y, "3D printing of shape memory polymer for functional part fabrication," The International Journal of Advanced Manufacturing Technology, vol. 84, no. 9–12, pp. 2079–2095, 2016.

[55]. Ge Q, Sakhaei AH, Lee H, Dunn CK, Fang NX, and Dunn ML, "Multimaterial 4D printing with tailorable shape memory polymers," Scientific Reports, vol. 6, p. 31110, 2016.

[56]. Ge Q, Dunn CK, Qi HJ, and Dunn ML, "Active origami by 4D printing," Smart Materials and Structures, vol. 23, no. 9, p. 094007, 2014.

[57]. Wu J, Yuan C, Ding Z, Isakov M, Mao Y, Wang T, Dunn ML, and Qi HJ, "Multi-shape active composites by 3D printing of digital shape memory polymers," Scientific Reports, vol. 6, p. 24224, 2016.

[58]. Qi HJ, Nguyen TD, Castro F, Yakacki CM, and Shandas R, "Finite deformation thermo-mechanical behavior of thermally induced shape memory polymers," Journal of the Mechanics and Physics of Solids, vol. 56, no. 5, pp. 1730–1751, 2008.

[59]. Yu K, Ritchie A, Mao Y, Dunn ML, and Qi HJ, "Controlled sequential shape changing components by 3D printing of shape memory polymer multimaterials," Procedia Iutam, vol. 12, pp. 193–203, 2015.

[60]. Mao Y, Ding Z, Yuan C, Ai S, Isakov M, Wu J, Wang T, Dunn ML, and Qi HJ, "3D printed reversible shape changing components with stimuli responsive materials," Scientific Reports, vol. 6, p. 24761, 2016.

[61]. Raviv D, Zhao W, McKnelly C, Papadopoulou A, Kadambi A, Shi B, Hirsch S, Dikovsky D, Zyracki M, Olguin C, et al., "Active printed materials for complex self-evolving deformations," Scientific Reports, vol. 4, p. 7422, 2014. [PubMed: 25522053]

[62]. Le Duigou A, Castro M, Bevan R, and Martin N, "3D printing of wood fibre biocomposites: From mechanical to actuation functionality," Materials & Design, vol. 96, pp. 106–114, 2016.

[63]. Zhang Q, Zhang K, and Hu G, "Smart three-dimensional lightweight structure triggered from a thin composite sheet via 3D printing technique," Scientific Reports, vol. 6, p. 22431, 2016.

[64]. Kamamichi N, Maeba T, Yamakita M, and Mukai T, "Fabrication of bucky gel actuator/sensor devices based on printing method," in Intelligent Robots and Systems, 2008. IROS 2008. IEEE/RSJ International Conference on. IEEE, 2008, pp. 582–587.

[65]. Cai J, Vanhorn A, Mullikin C, Stabach J, Alderman Z, and Zhou W, "4D printing of soft robotic facial muscles," in 26th International Solid Freeform Fabrication Symposium, 2015.

[66]. Peele BN, Wallin TJ, Zhao H, and Shepherd RF, "3D printing antagonistic systems of artificial muscle using projection stereolithography," Bioinspiration & Biomimetics, vol. 10, no. 5, p. 055003, 2015. [PubMed: 26353071]

[67]. Slightam JE and Gervasi VR, "Novel integrated fluid-power actuators for functional end-use components and systems via selective laser sintering nylon 12," in 23rd Ann Int Solid Freeform Fabrication Symp, 2012, pp. 197–211.

[68]. Bogue R, "3D printing: An emerging technology for sensor fabrication," Sensor Review, vol. 36, no. 4, pp. 333–338, 2016.

[69]. Ni Y, Ji R, Long K, Bu T, Chen K, and Zhuang S, "A review of 3D-printed sensors," Applied Spectroscopy Reviews, vol. 52, no. 7, pp. 623–652, 2017.

[70]. Muth JT, Vogt DM, Truby RL, Mengüç Y, Kolesky DB, Wood RJ, and Lewis JA, "Embedded 3D printing of strain sensors within highly stretchable elastomers," Advanced Materials, vol. 26, no. 36, pp. 6307–6312, 2014. [PubMed: 24934143]

[71]. Kesner SB and Howe RD, "Design principles for rapid prototyping forces sensors using 3-D printing," IEEE/ASME Transactions on Mechatronics, vol. 16, no. 5, pp. 866–870, 2011.

[72]. Yang Y and Chen Y, "Innovative design of embedded pressure and position sensors for soft actuators," IEEE Robotics and Automation Letters, vol. 3, no. 2, pp. 656–663, 2018.
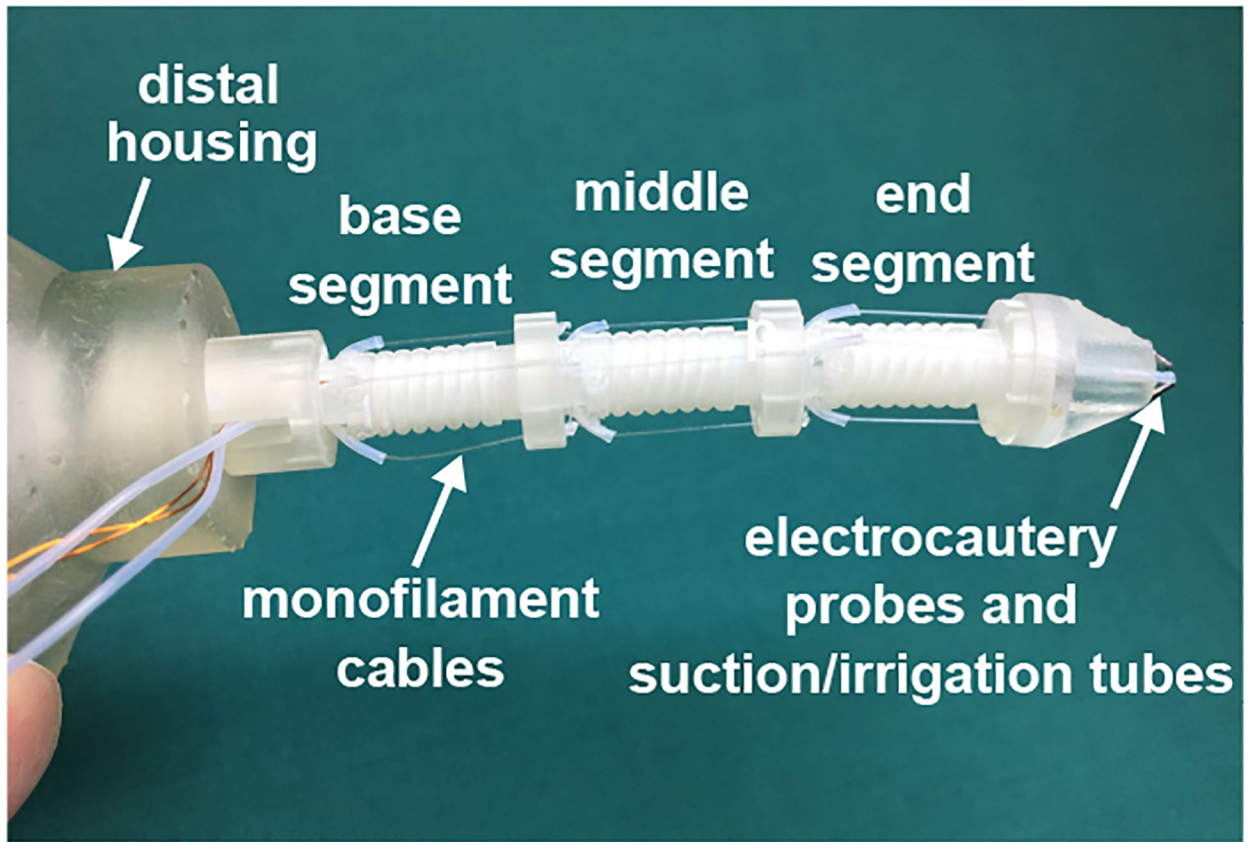
Author Manuscript

Author Manuscript

Author Manuscript

Author Manuscript

Fig. 1.
Three-segment MINIR-II robot equipped with electrocautery probes and suction/irrigation tubes.
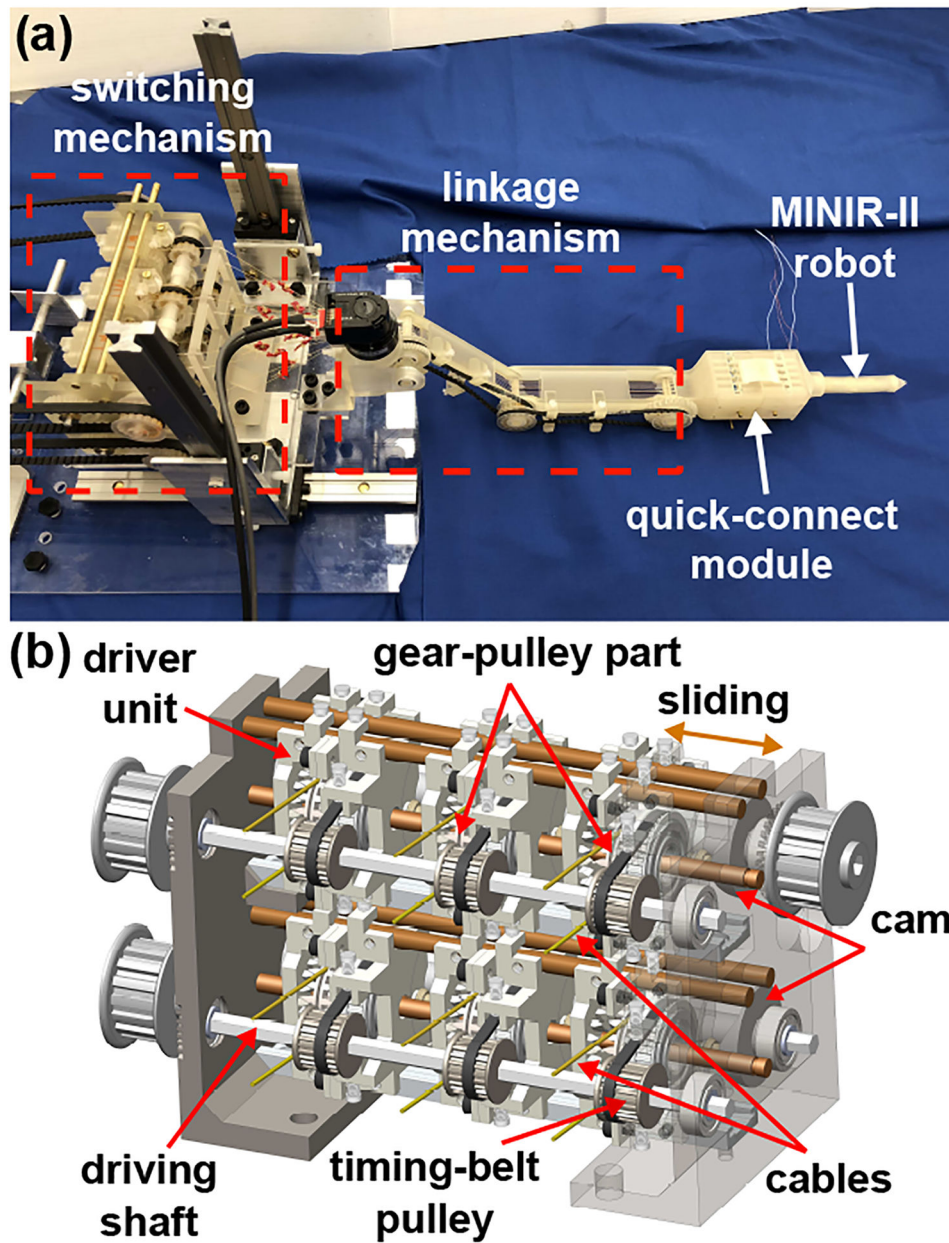
Fig. 2.
(a) MINIR-II robotic system consisting of the switching mechanism, linkage mechanism, and the quick-connect module. (b) Detailed CAD model of the switching mechanism.
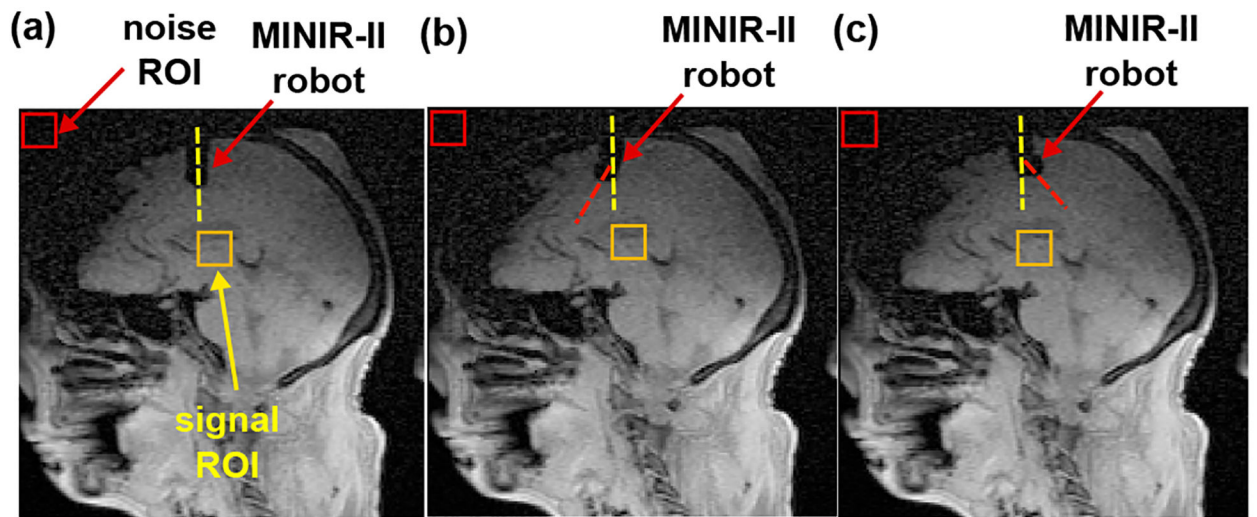
Fig. 3.
MR images showing the MINIR-II robot in the human cadaver study: (a) immediately after being inserted, (b) robot deflected rightward, and (c) robot deflected leftward.
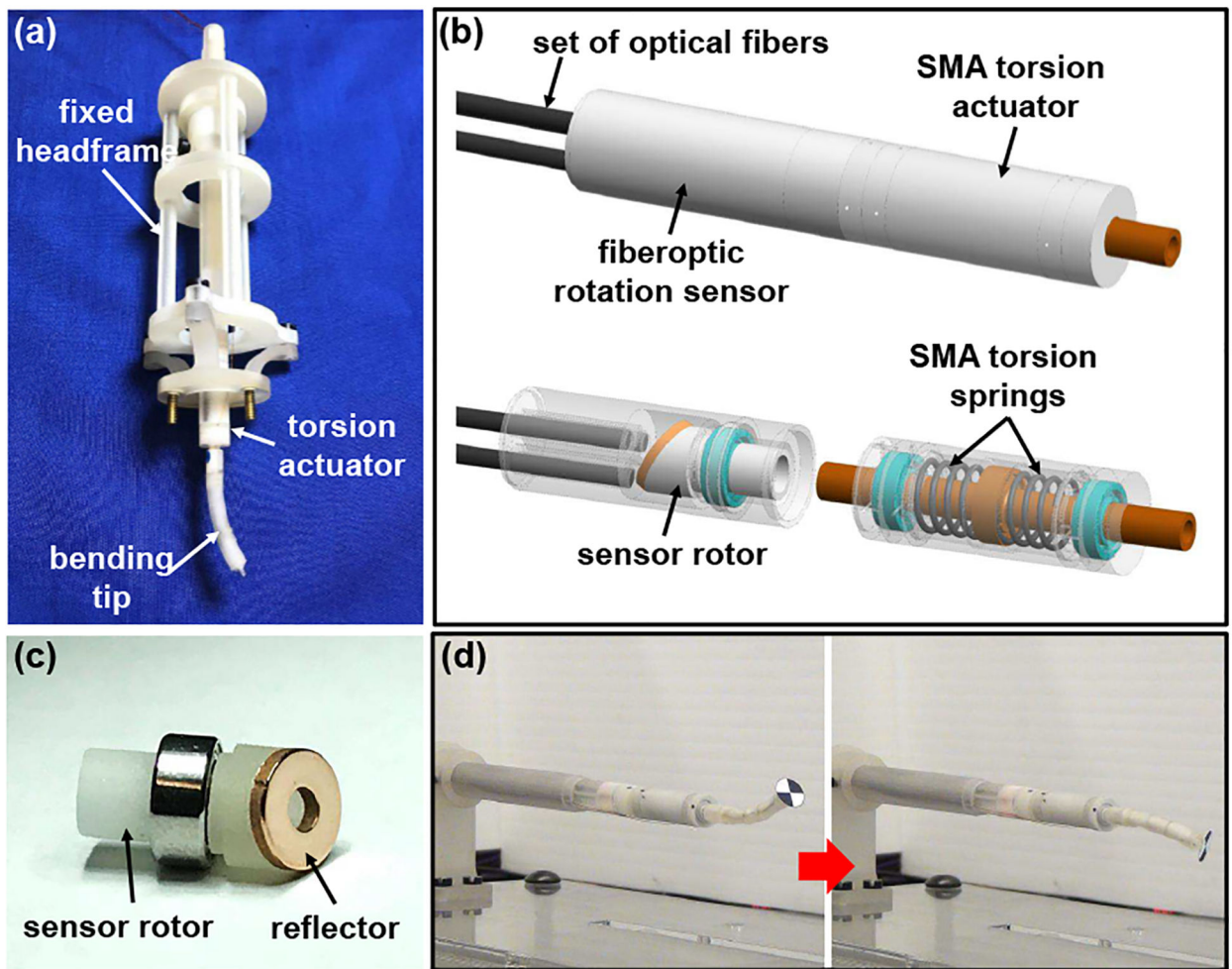
Fig. 4.
Development of the NICHE robot: (a) NICHE robot prototype mounted on a fixed headframe, (b) design of the SMA torsion actuator and fiberoptic rotation sensor, (c) prototype of the sensor rotor with the brass reflector, and (d) demonstration of tip articulation under feedback control.
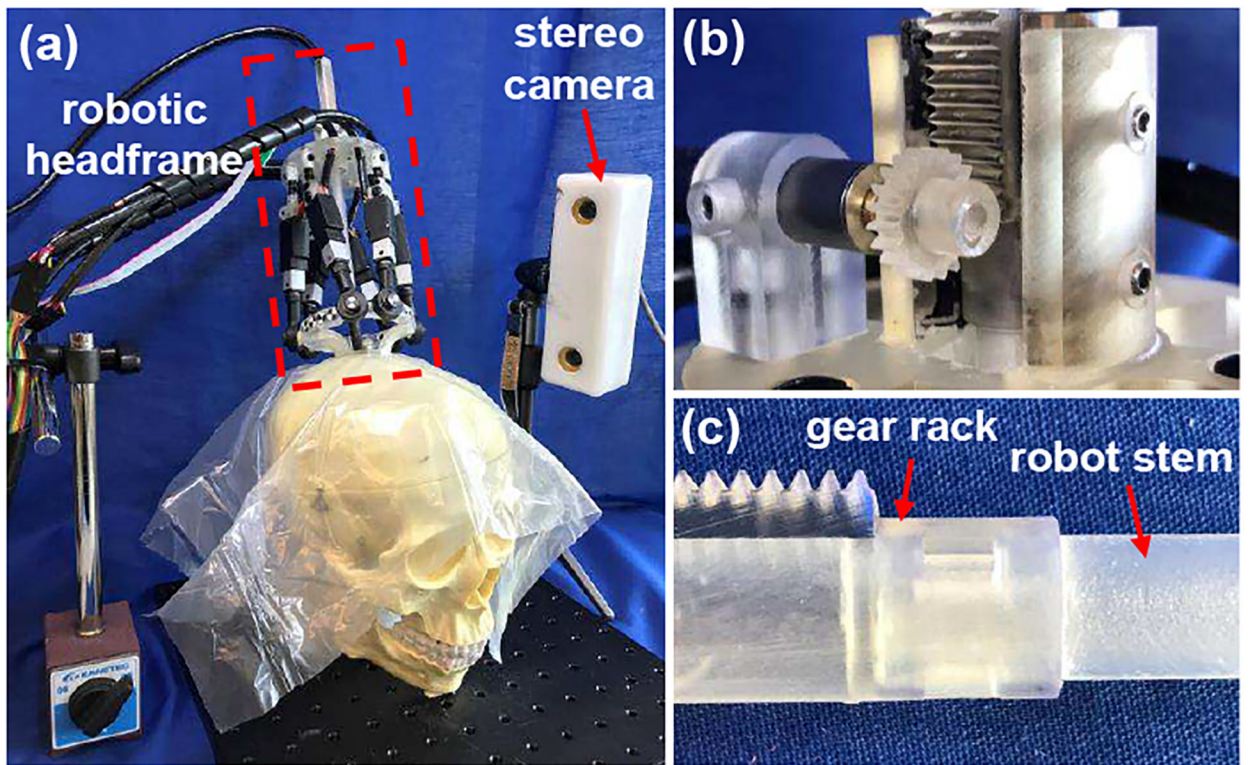
Fig. 5.
Skull-mounted robotic headframe: (a) demonstration of the headframe mounted on a skull model, (b) linear actuation module, (c) connection between the gear rack and robot stem via the snap-fit mechanism.
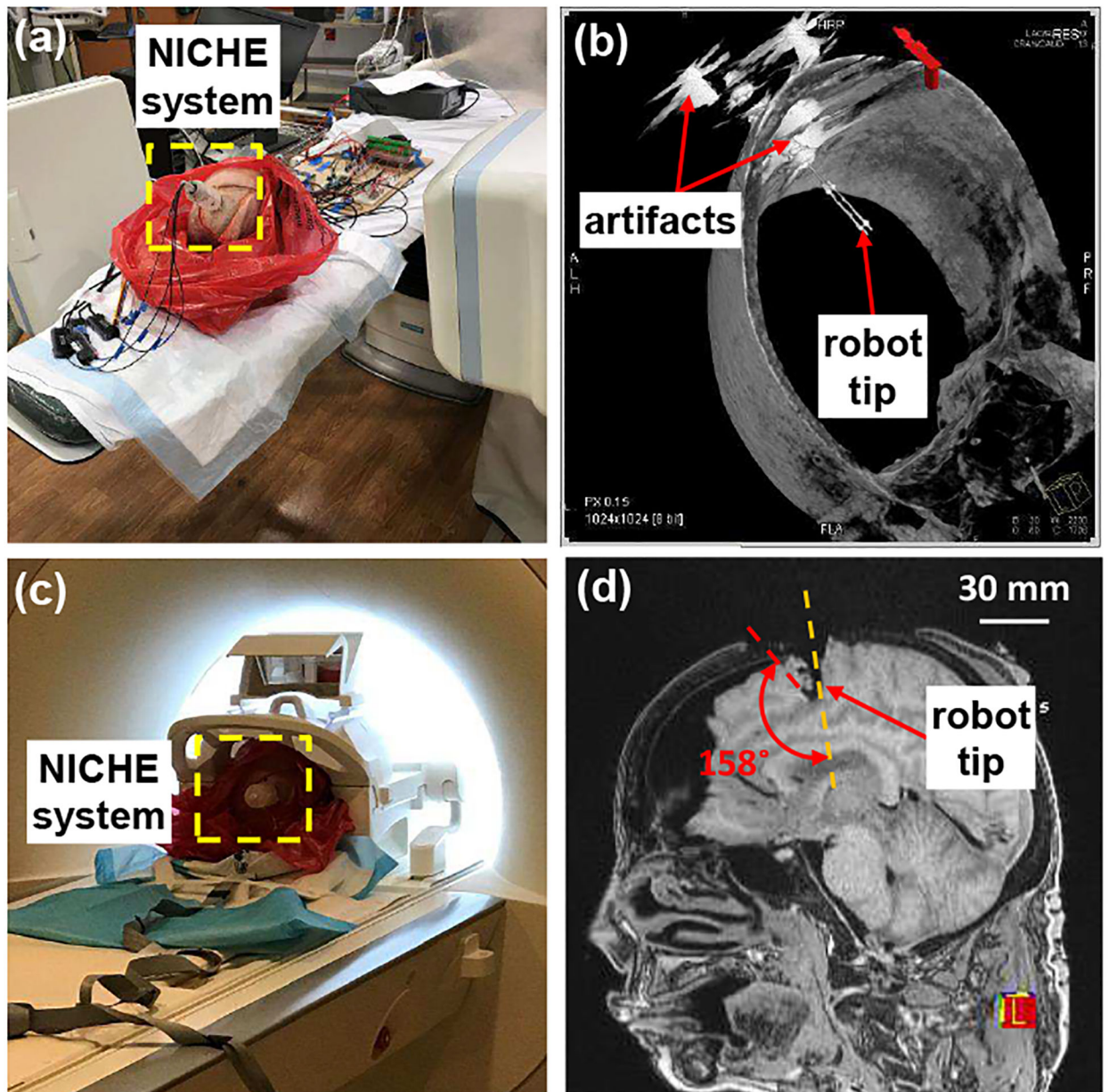
Fig. 6.
Ex vivo evaluation of the NICHE robot system using a human cadaver head: (a) setup for CT imaging-guided test, (b) 3D imaging reconstruction by the DynaCT technique, (c) setup for MR imaging-guided test, and (d) large-deflection of the robot tip in brain.
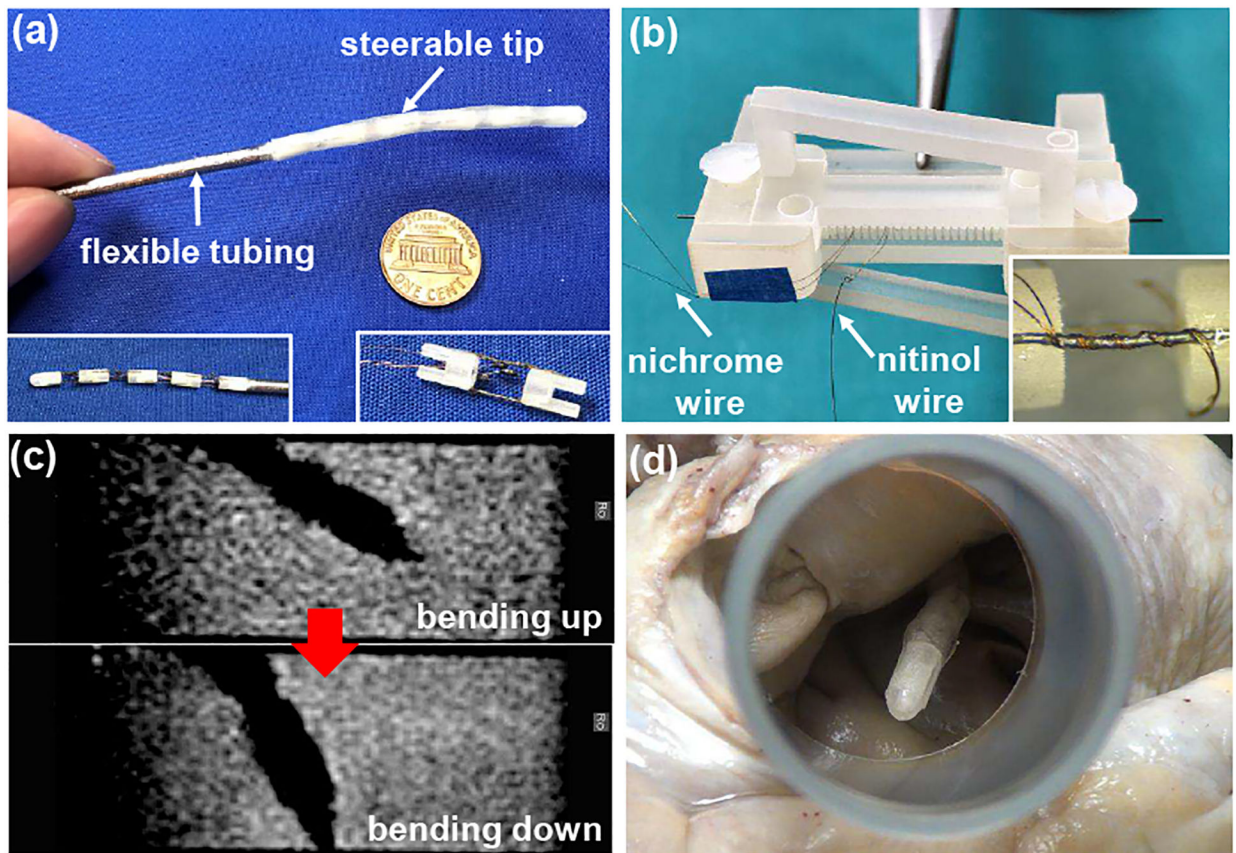
Fig. 7.
Development and evaluation of the robotic catheter for AFib treatment: (a) prototype of the robotic catheter, (b) routing nichrome coils around the SMA wire, (c) manipulation of the catheter tip under MR imaging guidance, and (d) *ex vivo* demonstration of the catheter using an explanted human heart.

Table I.

List of biocompatible 3D-printed materials.

Printing Technique	Materials (Manufacturers)	USP Class VI	ISO –10993	*Tensile Modulus (MPa)	*Tensile Strength (MPa)	*Glass Transition Temperature (°C)	*Heat Distortion Temperature @0.45 MPa (°C)
FDM	ABS-M30i, PC-ISO, ULTEM 1010 (Stratasys)	✓	✓	2190, 2000, 2770	36, 57, 81	108, 161, 215	96, 133, 216
	PEEK (3DGence, AON 3D, Apium P155, etc.)	✓	✓	4100	105	143	156 @ 1.8 MPa
SLA	Accure ClearVue (3D systems)	✓	-	2270–2640	46–53	62	51
	Somos Bioclear (DSM)	✓	✓	2770	50.4	43	50
	PA2200 (EOS) [18]	-	✓	1500–1800	45–52	176 (melting)	-
SLS	DuraForm PA (3D Systems)	✓	-	2586	43	-	180
IJP	VisiJet M2R-CL/WT (3D Systems)	✓	✓	1500–2000	35–45	-	51
	MED610/620 (Stratasys)	✓	-	2000–3000	50–65	52–54	45–50
	VisiJet M3 Crystal, VisiJet M3 Stoneplast,	✓	-	1463, 1850	42.4, 41	-	56,56
	VisiJet SL Clear, VisiJet M2R-GRY,	✓	-	2560, 1500–2000	52, 35–5	-	51, 51
	VisiJet M2R-TN, VisiJet CR-BK,	✓	-	2500–3000, 1800–2500	60–70, 37–48	-	71, 54–61
	VisiJet CR-CL 200, VisiJet CR-WT 200 (3D Systems)	✓	-	1400–2100, 1500–2000	30–3, 33–40	-	42–47

*
Multiple numbers correspond to multiple materials in the second column in the same row.

Table II.

List of 3D-printed unidirectional shape memory polymers.

technique	material	vendor or references
FDM	PLA, ABS, and Polyvinyl alcohol (PVA) DiAPLEX MM-4520 pellets	[52], [53] SMP Technologies, [54]
SLA	methacrylate-based solution	[55]
MJP	TangoBlack, VeroWhite, TangoBlack+, DM8530, DM9895	Stratasys, [56], [57]